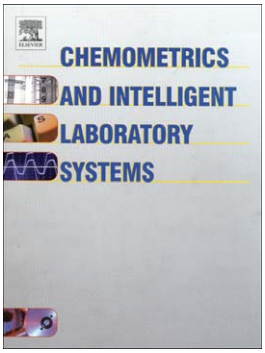

Efficient chemometric strategies for pet-pla discrimination in recycling plants using hyperspectral imaging

A. Ulrici, S. Serranti, C. Ferrari, D. Cesare, G. Foca, G. Bonifazi

PII: S0169-7439(13)00012-9
DOI: doi: 10.1016/j.chemolab.2013.01.001
Reference: CHEMOM 2597

To appear in: *Chemometrics and Intelligent Laboratory Systems*

Received date: 5 October 2012
Revised date: 6 December 2012
Accepted date: 8 January 2013

Please cite this article as: A. Ulrici, S. Serranti, C. Ferrari, D. Cesare, G. Foca, G. Bonifazi, Efficient chemometric strategies for pet-pla discrimination in recycling plants using hyperspectral imaging, *Chemometrics and Intelligent Laboratory Systems* (2013), doi: 10.1016/j.chemolab.2013.01.001

EFFICIENT CHEMOMETRIC STRATEGIES FOR PET-PLA DISCRIMINATION IN RECYCLING PLANTS USING HYPERSPECTRAL IMAGING

A. Ulrici [1], S. Serranti [2,*], C. Ferrari [1], D. Cesare [2], G. Foca [1], G. Bonifazi [2]

[1]*Dipartimento di Scienze della Vita, Università di Modena e Reggio Emilia, Padiglione Besta, Via Amendola 2, 42122 Reggio Emilia, Italy*

[2]*Dipartimento di Ingegneria Chimica Materiali Ambiente, Sapienza Università di Roma, Via Eudossiana 18, 00184, Roma, Italy*

* Corresponding Author: silvia.serranti@uniroma1.it

Telephone: +39 06 44585360; Fax: +3906 44585618

ABSTRACT

The effectiveness of Hyperspectral imaging (HSI) in the near infrared (NIR) range (1000-1700 nm) was evaluated to discriminate PET (polyethylene terephthalate) from PLA (poly(lactic acid)), two polymers commonly utilized as packaging for foodstuff, in order to improve their further recycling process. An internal calibration based on five reference materials was initially used to eliminate the variability existing among images, then Partial Least Squares-Discriminant Analysis (PLS-DA) was used to distinguish and classify the three classes, i.e., background, PET and PLA. Considering the high amount of data conveyed by the training image, the PLS-DA models were also calculated using as training set a reduced version of the original matrix, with the twofold aim to reduce the computational time and to deal with an equal number of spectra for each class, independently from the initial selected areas. A variable selection procedure by means of iPLS-DA was also applied on both the whole and the reduced matrix. The results obtained on the reduced matrix using only six variables provided a prediction efficiency higher than 98%. Moreover, the

possibility to recognize PET and PLA polymers by HSI in the NIR range was further confirmed by using Multivariate Curve Resolution (MCR) as an alternative approach, which also allowed to evaluate the effect of thickness of the transparent plastic samples.

KEYWORDS

hyperspectral imaging; feature selection; multivariate curve resolution; plastic recycling; polyethylene terephtalate (PET); polylactic acid (PLA).

1. INTRODUCTION

HyperSpectral Imaging (HSI), also known as chemical or spectroscopic imaging, represents an emerging technique that provides both the spatial information characteristic of imaging methods and the spectral information typical of spectroscopy [1]. Compared to traditional spectroscopic techniques, the HSI allows to acquire spectral data in correspondence to every single pixel of an image; in this way, it enables the visualization of the chemical composition of the sample retaining, at the same time, the advantages of being fast, non-destructive and of not requiring chemicals. In the literature, a number of possible applications of HSI have been already presented, mostly in the fields of food [2-4], pharmaceutical industry [5] and medicine [6]. In addition, since multivariate analysis tools are mandatory to extract the significant physical-chemical information from hyperspectral images, various research works describing chemometric approaches developed to solve HSI-related issues recently appeared [7-9].

Thanks to the high spatial and spectral resolution values that can be reached, HSI allows to collect a wide amount of data in very short times, providing single hyperspectral images with file sizes of about 50 MB and more. If on the one hand, the large amount of hyperspectral data represents the main advantage of HSI technique, on the other hand, the corresponding high

computational load of high dimensional data, which is also known as the *curse* of dimensionality [10], is a key issue. A proper data size reduction able to speed up the processing, but preserving the useful information to perform a reliable analysis, thus represents a fundamental concern in the HSI context. Data dimensionality reduction is a key-point, firstly during the image analysis stage, through the elaboration of strategies able to facilitate the data handling, and secondly for the development of efficient industrial *on-line* applications – when it is necessary to follow real-time processes – through the application, for instance, of feature selection methods such as interval Partial Least Square (iPLS) [11] and/or Genetic Algorithms (GA) [12].

A further problem that has to be faced when dealing with hyperspectral imaging is related to the standardization of the instrumental response. In fact, the possible variations in the experimental setup including, for instance, camera inconsistencies, variations of the illumination conditions and changes in power or temperature which may cause a drift of the signal over time, can heavily affects the quality of the hyperspectral images [13] and, as consequence, the further processing and the related results. To address this issue, Burger and Geladi [14] developed a procedure to render the image quality independent from the acquisition setup. In particular, in addition to an optimization of the external calibration normally used to convert the raw images into reflectance images, they further processed the hyperspectral images by means of an internal calibration procedure, aimed to improve the reproducibility of the system over time.

As far as the analysis of waste materials is concerned, some works have already shown the usefulness of HSI techniques in sorting solid materials such as paper [15], glass [16], car-fluff [17], bottom ash [18], compost [19] and polymers [20-23].

The increasing need to reduce the impact of plastic waste on the environment has led to the development of biodegradable polymers. Among them, poly(lactic acid) (PLA) is becoming widely used and nowadays represents an interesting environmentally-friendly alternative to polyethylene terephthalate (PET) since, being entirely made from corn or sugarcane, it is fully biodegradable and compostable. PLA is a thermoplastic aliphatic polyester that is obtained from renewable resources

(e.g. corn starch, tapioca roots, chips or starch, sugarcane, etc.). PET is a thermoplastic polymer resin, of the polyester family. It is utilized to produce synthetic fibers, beverage and other liquid containers, food packaging, etc.

As PLA has a similar appearance as well as similar density to PET, the use of PLA for packaging materials such as food containers and bottles, and in films also for packaging is continuously increasing. However, the fact that its aspect is very similar to that of PET is posing serious problems to the recycling stream of this latter polymer, since consumers tend to erroneously put PLA packages into the recycling bins for plastic materials. Since the potential contamination of PLA in the PET recycling stream can have a negative impact on the physical properties (e.g., on molecular weight) of extruded rPET [24, 25], the sorting of these two polymers is an outstanding concern in recycling industry. PLA and PET can be utilized as food packaging in transparent and/or expanded forms, the latter one resulting from specific processing where air is added and embedded in the polymeric structure to originate a cellular structure. Both transparent and expanded PET and PLA, even if different from a polymeric point of view, are quite similar in terms of commonly detectable physical attributes and appearance, strongly conditioning the possibility to perform a simple “human” and/or “automatic” recognition.

The present study was thus addressed to define a new method that can be implemented for the sorting of the two polymers so that they can follow different recycling routes, being PLA biodegradable, whereas PET can be mechanically recycled. The use of HSI in the near infrared (NIR) range could be of great help to discriminate these two polymers and to the best of our knowledge this is the first study on using HSI to solve this problem.

Firstly, in order to minimize the uninformative variability existing among the different reflectance images, a transfer calibration based on five reference materials was applied, where the optimal polynomial order of the transfer function was also determined. Afterwards, several chemometric methods have been used for the analysis of PLA and PET sample images, including Principal Component Analysis (PCA), Partial Least Squares-Discriminant Analysis (PLS-DA) [26],

interval PLS-DA (iPLS-DA) [11] and Multivariate Curve Resolution (MCR) [27]. Particular attention has been paid to the development of strategies aimed to minimize the dimension of the analyzed data: a compression strategy, operating both pixel-wise and wavelength-wise, was developed to reduce the size of the original training image (118400 pixels × 98 wavelengths) to a reduced matrix (600 pixels × 6 wavelengths). Analogous classification results were obtained with the original dataset and with the reduced matrix.

2. MATERIALS AND METHODS

2.1. Samples and data collection

2.1.1. Samples

The analysed PET and PLA samples, in both transparent and expanded forms, have been provided by Coopbox (Bibbiano, Reggio Emilia, Italy), a leading food packaging producer in Italy and Europe. They are constituted by trays (or tray portions, e.g.: bottom and/or cover of the trays), commonly used as fresh food packaging as well as by the corresponding flakes, obtained after tray milling. The measured thickness of the samples were 0.2 mm for transparent PLA (t-PLA), 0.3 mm for transparent PET (t-PET), 0.9 mm for expanded PLA (e-PLA) and 1.0 mm for expanded PET (e-PET).

2.1.2. Hyperspectral imaging system

NIR hyperspectral images were acquired using a NIR Spectral Camera™ (Specim, Finland), embedding an ImSpector N17E™ imaging spectrograph working in the spectral range from 1000 to 1700 nm, coupled with a Te-cooled InGaAs photodiode array sensor (320 × 240 pixels) with pixel resolution of 12 bits. The spectrometer was coupled to a 15 mm lens. The spectral resolution of the

hyperspectral imaging system was 7 nm. The pixel size was around 0.6x0.6 mm. The illumination system is constituted by a diffused light cylinder source, aluminum internal coated, embedding five halogen lamps producing a continuous spectrum signal optimized for spectra acquisition in the NIR wavelength range.

The utilized hyperspectral imaging based platform (DV Srl, Italy) was equipped with a conveyor belt (width = 26 cm and length = 160 cm) allowing to carry out experiments on particle flow streams in order to perform, at a laboratory scale, *on-line* detection of particles in a sorting and/or quality control perspective. The pushbroom configuration of the imaging system, consisting in the line by line image acquisition, represents the optimal solution for possible *on-line* industrial applications.

2.1.3. Image acquisition and calculation of reflectance values

Hyperspectral images of PET and PLA samples were acquired, generating data hypercubes having 320 pixels per row and a number of rows varying from 300 to 370 depending on the acquired image sample field. Due to the low S/N ratio characterizing the measurements at the extremities of the covered spectral range, only the 98 wavelengths between 1006 and 1685 nm were considered for further data analysis.

Image acquisition was carried out according to a sample acquisition scheme defined after preliminary tests. The setup used for the acquisition of all the images was composed by different parts: a silicon carbide (SiC) sandpaper sheet used as background and covering the whole image field, a high-reflectance white ceramic tile as the standard reference, three square pieces of painted surfaces with different grey-scale tones as additional reference materials, and an additional square white tile having a sample-support function. The use of an inorganic high-reflectance material as sample-support allowed to improve the light absorption of transparent polymer samples – that is very low considering the polymer thickness – by taking advantage both from the direct incident

beam and from the light reflected back by the white tile. It should be underlined that all the materials described above showed in the acquired spectral range very "flat" spectra, i.e. almost constant reflectance values, diverging only in the reflectance levels.

Firstly, an image of the acquisition sample-support setup without the plastic samples (*Img0*) was acquired to be used as reference image in the further image correction step. Afterwards, 10 images of PET and PLA samples were acquired as follows:

- *Img1-Img3*: 3 images representative of PET and PLA tray samples, both transparent and expanded. The different tray samples were disposed in different positions in the images in order to verify that no effects due to possible spatial variations in the system response were present;
- *Img4*: tray samples of the two transparent polymers were imaged in single layer as well as considering two, three and four overlapped layers, with the specific aim to evaluate the possible effect of polymer thickness;
- *Img5-Img6*: flakes samples of both transparent and expanded PET and PLA arranged in rows were imaged. The spatial disposition of the different rows was changed in the two images;
- *Img7-Img10*: both tray and flakes samples of both polymers were acquired in different "overlapping" combinations, in a way to simulate sample distributions more similar to real cases occurring in a recycling plant.

All the images were composed by 370 pixel rows and 320 pixel columns, except for Img2, Img3, Img6 and Img7, which were composed by 300 pixel rows and 320 pixel columns. The acquisition scheme, the corresponding RGB image and results of elaborations of the HSI images of at least one member of each group listed above are reported in the following figures: Figure 3 (Img1), Figure 6 (Img7 and Img9) and Figure 8 (Img4 and Img5).

The raw images were converted to reflectance values applying a simple external calibration based on the high-reflectance standard reference and on the dark current measured by covering the camera lens with its cap, according to the following equation:

$$R_{(i,\lambda)} = \frac{C_{i,\lambda} - D_{i,\lambda}}{W_{i,\lambda} - D_{i,\lambda}} \qquad \text{(eq. 1)}$$

where $R_{i,\lambda}$ are the calculated reflectance values, $C_{i,\lambda}$ are the measured intensity values of the raw image, $D_{i,\lambda}$ are the dark current intensity values and $W_{i,\lambda}$ are the high-reflectance standard reference intensity values, measured for each one of the i row pixels and of the λ wavelengths.

2.2. Data pre-processing and analysis

2.2.1. Image correction by internal calibration

The reduction of the variability among images over time, which is mainly due to instrumental instability, is essential for the quality and reliability of the further analysis, since it allows working with merged images and/or to apply models calculated on a single image to the others. The calibration step used to transform the raw data into reflectance values, described in paragraph 2.1.3, was not sufficient to completely eliminate the variability among images, as verified by applying PCA to merged images (mean centered spectra). As an example, the results of the analysis performed on Img0 and Img1 merged together are shown in Figure 1 (a, b), where it can be seen that the two clusters corresponding to the two images are clearly distinguishable both on the PC1-PC2 scores plot (Figure 1a) and on the PC2 score image (Figure 1b). As proposed by Burger & Geladi [14], a possible solution to this issue can be achieved by including a grayscale series of internal standards in the field of view of each image and then using the median spectra calculated for each of them to individually correct the different hypercubes, called “slave”, to match a previously defined “master” hypercube. In the cited paper, the effect of correction models based on

single-point stretch, multi-point linear as well as second order quadratic regression was evaluated, concluding that the latter one was the most effective correction method.

In the present work, for each image a random sampling procedure was used to divide into three groups the pixels included in each region of interest (ROI) selected accordingly with each one of the five reference materials (i.e., the high-reflectance standard, the three square pieces of painted surfaces, and the white sample-support tile). For each pixel group, the median spectrum was calculated and then included in a matrix of reference spectra that was finally composed by (3 median spectra) × (5 reference materials) = 15 spectra. The decision to use more than a single median spectrum for each ROI was taken in order to consider the effect of possible spatial variability of the reference materials, also considering that four out of five of them were not calibrated standards. The internal calibration step was carried out by computing a regression model between the reference spectra of Img0, taken as the master image (Y), and the reference spectra of each one of the "slave" images (X), wavelength by wavelength.

In order to select the most appropriate order of the regression model, the values of the first-, second- and third-order regression coefficients were estimated, together with the corresponding statistical significances. By repeating the whole procedure 15 times for each order of the regression model, we observed that only the linear regression models always led to statistically significant regression coefficients. For this reason, the correction of all the images was carried out by applying a set of linear regression models, according to the equation:

$$C(I,\lambda) = \beta_0(I,\lambda) + \beta_1(I,\lambda) \times R(I,\lambda) \qquad \text{(eq. 2)}$$

where C(I,λ) is the corrected reflectance value, R(I,λ) is the original reflectance value, and β_0(I,λ) and β_1(I,λ) are the regression coefficients, calculated using the reference spectra for each image I at each wavelength λ.

The comparison of the PC1-PC2 scores plots obtained before (Figure 1a) and after (Figure 1c) applying the correction by internal calibration with the regression model of equation 2, as well as the comparison of the corresponding PC2 score images (Figures 1b and 1d, respectively) demonstrate the effectiveness of the proposed procedure.

2.2.2. Explorative analysis and definition of the classes

The corrected hyperspectral images were individually subjected to an explorative analysis by means of PCA. Several preprocessing methods including detrend, standard normal variate, first and second derivatives, normalization and mean centering were evaluated both separately and in different combinations; among them, 2^{nd} derivative (15 points window) combined with mean centering was chosen as the one leading to the best results. In order to shown how the pretreatment works, the raw median spectra of the three classes and the corresponding preprocessed ones are reported in Figure 2.

By looking at the PCA score images of Img1, three classes were defined for the subsequent classification purposes: background, PET and PLA. Background was defined as a separate class, considering the whole scene area in the classification step, without performing any masking/segmentation of the images. This choice was made in order to clearly separate the contribution of the reflectance from the white sample-support tile from that of transparent samples. In addition, in the PET and PLA classes both the transparent and the expanded forms of each polymer were grouped together, since we focused on the identification of PET and PLA samples based on their chemical composition, independently of their physical form. By the way, the separation of transparent and expanded samples can be easily achieved by means of simpler systems, e.g., RGB imaging devices.

2.2.3. PLS-DA classification

Partial Least Squares-Discriminant Analysis (PLS-DA) [26] was used to discriminate the three classes, using the preprocessing method defined in the explorative analysis phase. The optimal dimensionality of the PLS-DA classification models was defined by considering the minimum Root Mean Square Error estimated in the Cross-Validation (RMSECV). Contiguous-blocks cross-validation with 10 deletion groups was chosen in order to consider neighboring pixels in the same deletion group. Img1 was used as training set, while Img2-Img6 were used as external test sets to quantitatively evaluate the predictive ability of the calculated classification models. The classification results for these images are reported in terms of Efficiency %, i.e. the geometric mean of the Sensitivity and Specificity values [28]. Due to the fact that in the remainder images (Img7-Img10) the PLA and PET polymer samples were overlapped each other, for these ones it was not possible to evaluate quantitatively the predictive performance of the classification models. Therefore, in this case the effectiveness of the discriminant models was evaluated only qualitatively by looking at the pseudo-color images of the predicted class probability values and by comparing these with the corresponding acquisition scheme.

2.2.4. Calculation of reduced matrices

Considering the high amount of data contained in the training set image (size of Img1: 118400 single pixel spectra × 98 wavelengths), the PLS-DA models were also calculated using as training set a reduced version of the original data matrix, in order to test whether it was possible to obtain the same classification performances, but drastically lowering the time needed for model computation. The reduced matrix was calculated for Img1 by using the following procedure:

- for the ROI corresponding to each class, subdivide the *n* pixels in *n*/25 groups;
- for each group, calculate the mean spectrum;
- randomly select 200 mean spectra

- create the reduced matrix with 200 mean spectra for each class (total size: 600 mean spectra × 98 wavelengths)

In this case, a "customized" cross-validation with 10 deletion groups was used, where each group contained 20 spectra for each class.

2.2.5. Variable selection by means of iPLS-DA

Since in the NIR hyperspectral images the variables (i.e., the reflectance values at the different spectral wavelengths) are highly collinear, variable selection represents an important step to decrease the computational load as well as to increase the robustness of the prediction models [10]. Among the several existing methods for variable selection [29], in the present work the simple but effective iPLS-DA algorithm was applied. As described in [11], iPLS-DA, that is a modification of the interval-PLS algorithm applied to classification tasks, works by dividing the full-spectrum in intervals of equal width and calculating classification models for each one of these spectral regions. In the forward-selection mode, the best interval is then chosen as the one leading to the minimum value of RMSECV. Then, two-intervals models are built by adding each one of the remainder intervals to the previously selected one. Once again, the model showing the lowest RMSECV value is selected and this iterative procedure is repeated until no significant improvement of RMSECV is achieved. Conversely, in the reverse-selection mode, the intervals are iteratively removed according to a decrease in the RMSECV value. Since this latter procedure is more conservative than the former one, i.e., a larger number of wavelengths are usually preserved in the final model, the forward-selection mode was used in the present work.

In particular, forward iPLS-DA was applied to Img1 as well as to the corresponding reduced matrix considering different numbers of intervals, i.e. 7, 14 and 49 intervals, corresponding to window sizes equal to 14, 7 and 2 variables, respectively. The same preprocessing and cross-validation procedures used for the calculation of the PLS-DA models on the whole signals were

applied. Also in this case, Img1 was used as training set, and the remainder images were used to evaluate the predictive capability of the selected models, as it was previously describes in section 2.2.3.

2.2.6. Multivariate Curve Resolution

Considering the spectroscopic nature of the NIR hyperspectral images, an alternative approach for mapping the sample constituents is represented by the so-called resolution methods. Among them, Multivariate Curve Resolution (MCR) is the most popular one in the frame of multivariate image analysis [30]. Based on the Lambert-Beer law, MCR aims to decompose the original unfolded hypercube matrix into two matrices, the first one containing the spectra recovered for the pure chemical components, and the second one with the corresponding concentration profiles for each pixel of the image. In particular, by means of an optimisation procedure based on Alternating Least Squares (ALS), MCR works decomposing a matrix of spectra according to the matrix equation:

$$X = CS^{\mathrm{T}} + E \qquad \text{(eq. 3)}$$

where X represents the unfolded data matrix, S the pure component spectra, C their corresponding concentrations and E the matrix of the residuals. In the same way as PCA is used to have a visualization of the score images, MCR is allows represent the distribution maps of each component, which are obtained by refolding the corresponding concentration vector. Furthermore, this method allows the reduction of the remarkable hypercube dimensions to just few chemically meaningful pure components [10].

Despite the advantages offered this approach, mainly concerning the ease of interpretation of the results in chemical terms, MCR is affected by a drawback: several solutions may contemporarily exist for the matrix decomposition, i.e., several pairs of C and S^T matrices [30]. In order to reduce this ambiguity, various constraints may be applied in a manner to induce the ALS optimization to

converge towards the correct solution. Among them, the most common one is the non-negativity constraint, that can be set both for the pure components spectra and for the concentration values.

Concerning the analysis of the polymer images, a MCR model was calculated on the reduced matrix of Img1, using the median spectra of the classes as initial guesses and non-negativity constraints for both C and S. Additionally, spectra normalization to unit area was used. The obtained MCR model was validated using Img2-Img10 as test set, with the aim to get the distribution maps of the different imaged components. The results were qualitatively evaluated by comparing the distribution maps with the corresponding acquisition schemes.

3. RESULTS AND DISCUSSION

3.1. Explorative analysis and class definition

Before calculating the classification models, all the hyperspectral images were subjected to exploratory analysis by means of PCA. No cleaning step was usually required; only in the case of Img3 the removal few outlier pixels has been necessary (19 out of 118400).

Considering only the images where the polymers were not overlapped, i.e., Img1-Img6, the number of significant PCs always resulted equal to 2 (accounting for about 90% of the total variance), therefore the pixel clusters identified in the corresponding PC1-PC2 scores plot were used to define the three classes: background, PLA and PET. Figure 3 reports the RGB image corresponding to Img1 (Figure 3a), the PC1-PC2 scores plot of Img1 used for class definition, where the clusters corresponding to the three classes are highlighted with different colours (Figure 3b), and the corresponding image representation of the three selected classes (Figure 3c). In order to better interpret the results of PCA, the relationships between the pretreated median spectra of PET and PLA and the PCA loadings were evaluated. Linear correlations between PC1 loadings and the pretreated median spectrum of PET (Figure 4a) as well as between PC2 loadings and the pretreated

median sprectrum of PLA (Figure 4b) were found, confirming that PC1 fundamentally reflects the variability due to the PET-related spectral features, while PC2 is mainly related to the PLA ones. Moreover it can be noticed that in the scores plot (Figure 3b), the cluster corresponding to the transparent PLA sample is located between PLA and background clusters. Plausibly, the very low thickness of the transparent PLA sample led to a significant contribution of the underlying white tile to the spectra of transparent PLA.

3.2. PLS-DA results

The optimal dimensionality of the PLS-DA classification model, corresponding to the minimum error in cross-validation, was equal to 2 Latent Variables. The classification results are reported in Table 1, where the cross-validation results obtained on the training image (Img1) perfectly agree with those obtained for the external prediction of the test images. In general, values in prediction higher than 98% were obtained for all the classes in all the five test images.

The same approach was applied using as training set the Img1 reduced matrix of 600 spectra. Also in this case a model with 2 Latent Variables was selected by cross-validation. As reported in Table 1 the results obtained on the reduced matrix are absolutely comparable to those obtained on the original dataset, but the time needed for model calculation has been shortened from about 150 seconds to just about 10 seconds. Furthermore, it should be noticed that using this approach, an equal number of spectra is used for each class, independently of the size of the selected areas.

3.3. Classification results after variable selection

The forward iPLS-DA algorithm for variable selection, that was applied using 7, 14 and 49 intervals, led to the selection of the wavelength regions shown in Figures 5b and 5c, for the whole and the reduced matrices of Img1, respectively. For comparison purposes, Figure 5a reports the Variable Importance in Projection (VIP) scores of the PLS-DA model calculated on the whole

matrix and considering the entire spectral range. VIP scores estimate the importance of each variable used in a PLS model, so that they are often used as a criterion for effective variable selection [31]. Generally, the criterion adopted to determine whether a certain variable is actually significant is the 'greater than one rule', which derives from the fact that the average of squared VIP scores equals 1. For this reason, in Figure 5a the horizontal dashed line reports the threshold value equal to 1.

As stated by Andersen & Bro [32], the use of variable selection methods is generally addressed to reach three principal goals: i) the decrease of the computational time for model application; ii) the deletion of irrelevant, noisy or unreliable variables that may reduce the model predictions; iii) the possibility to find a chemical meaning for the interpretation of the model results. In the present work, variable selection has gained the goal to decrease the computational time of about 90% (Tab. 2). On the other hand, the results obtained after variable selection are definitely comparable to those obtained before, which were already close to 100% in Efficiency. Moreover, it must be stressed out that the introduction of the reduced matrix has proven to be a good solution for the classification of polymers using HSI, also in conjunction with feature selection. In fact, feature selection performed on the reduced matrix always allowed to obtain models with a number of variables lower than the number selected with the corresponding whole matrix, and with prediction performances analogous to those obtained on the whole matrix. Indeed, for all the three classes and for all the test images, Classification Efficiency values higher than 98% were always obtained. In particular, two models calculated on the reduced matrix seem particularly promising by a practical point of view:

- the classification model obtained with iPLS-DA using an interval size equal to 2, which led to the selection of only 6 wavelengths (1034, 1041, 1440, 1447, 1636 and 1643 nm) giving an average Efficiency value in prediction equal to 99.81 % (overall best performing model);
- the classification model obtained with iPLS-DA using an interval size equal to 7, which led to the selection of 7 contiguous wavelengths (1594, 1601, 1608, 1615, 1622, 1629 and 1636 nm) giving an average Efficiency value in prediction equal to 99.69 %;

In general, a very good correspondence was observed among the spectral regions selected using the different iPLS-DA interval sizes on the same matrix, as well as comparing the selection performed on the two matrices. In particular, the spectral region between 1600 and 1650 nm resulted to be the most significant one, since it was always selected on both the matrices and indipendently of the interval size, in agreement with the VIP scores obtained by PLS-DA before variable selection. In this spectral region the main absorption band is due to the first overtone of the C-H stretching [15, 33]. What is more, one of the two best performing models allowed to obtain optimal classification results using only wavelengths falling in this range. This result is interesting by a practical point of view and also reasonable, since between PET and PLA polymer structures there are many differences concerning the nature and number of the C-H bonds.

Finally, Figure 6 reports the prediction results for the test images Img7 and Img9, obtained with the overall best performing model, calculated using the reduced matrix and the smallest number of selected variables (last column of Table 2). As shown by the predicted probability images (Figure 6c), the model based on 6 wavelengths only was able to clearly distinguish the three classes although the very low sample thicknesses. In particular, it can be noticed that both e-PLA and e-PET flakes were distinctly assigned to the respective classes, while the overlapped t-PLA and t-PET flakes were correctly indicated as belonging to both the polymer classes (cyan colour is intermediate between green for PET and blue for PLA) since the corresponding pixel spectra reflected the composition of both polymers.

3.4. Multivariate Curve Resolution results

The median spectra of the classes background, PLA and PET used as initial guesses for the calculation of the MCR-ALS model were calculated on the reduced matrix and resulted to be almost identical to the corresponding median spectra calculated on the whole Img1 (Figure 2a). The spectra profiles of the three components recovered by means of MCR-ALS are reported in Figure 7.

As shown by the pseudo-color distribution images of Img4 and Img5 (Figure 8c) as well as of Img7 and Img9 (Figure 6d), that were built by superimposing the distribution maps of the three components , the MCR model is clearly able to distinguish the two polymers in all the images used as test sets.

With respect to Img4 (Figure 8c), that was set up to evaluate the effect of the sample thickness on discrimination, the pseudo-color image obtained shows that no variations can be noticed among different thicknesses for PET samples. On the other hand, in the case of PLA, the single layer sample is perceived as a combination of PLA and of the white tile underneath, while starting from the double layer sample, only the PLA contribute can be observed. Out of seven test images, only a partial misclassification of the e-PET tray sample in Img8 was observed, were only few pixels were identified as belonging to the backgroundclass. Similar results can be observed for Img9 (Figure 6d), where the t-PLA was imaged together with the PET flakes.

Although, when compared with PLS-DA, MCR-ALS represents a more explorative and non discriminant-oriented method, the results obtained using these two independent approaches were perfectly in agreement.

4. CONCLUSIONS

A NIR-HSI system operating in the spectral range between 1000 and 1700 nm was used to effectively classify and spatially distinguish samples of PET and PLA, two polymers that need to be sorted and separated in recycling plants. With the aim to improve the reproducibility of the images over time, particular attention has been paid to the image correction step. The use of an internal calibration step based on five reference materials was proved to be very useful, in addition to the normal reflectance calibration based only on the dark current and on a high reflectance standard. Furthermore, the use of a reduced matrix having dimension {600x98} as training set for the

calculation of the PLS-DA model allowed to obtain Classification Efficiency values in prediction higher than 98% and absolutely comparable to those obtained using the original {118400x98} training image. This strategy is thus effective to facilitate the data handling and, at the same time, to significantly reduce the computational load and time needed for the image analysis. This was also confirmed in the iPLS-DA variable selection step, where the use of the reduced matrix allowed a decrease of the computational time of about 90% and a selection of a lower number of variables compared to the whole matrix. The Classification Efficiency values estimated in prediction using the PLS-DA model calculated on the reduced matrix using only 6 variables were higher than 98%. The effectiveness of the hyperspectral imaging system for distinguishing the two polymers, both in transparent and expanded physical forms, was also confirmed by using a different approach, i.e., applying MCR-ALS to the reduced matrix. The results obtained with MCR-ALS were in perfect agreement with those obtained with PLS-DA.

5. ACKNOWLEDGEMENTS

Coopbox Italia Srl (Via Gandhi, 8 42100 Reggio Emilia, Italy) is acknowledged for furnishing the PET and PLA samples used for this study.

6. REFERENCES

1. H. Grahn, P. Geladi (Eds.), Techniques and Applications of Hyperspectral Image Analysis, John Wiley & Sons, Ltd., Chichester, 2007.

2. A.A. Gowen, C.P.O'Donnell, P.J. Cullen, G. Downey, J.M. Frias, Hyperspectral imaging – an emerging process analytical tool for food quality and safety control, Trends Food Sci. Tech. 18 (2007) 590-598.

3. Sun, D-W. (Ed.), Hyperspectral imaging for food quality analysis and control, Academic Press/Elsevier Ed., San Diego CA, 2010.

4. A. Del Fiore, M. Reverberi, A. Ricelli, F. Pinzari, S. Serranti, A.A. Fabbri, G. Bonifazi, C. Fanelli, Early detection of toxigenic Fungi on maize by hyperspectral imaging analysis, Int. J. Food Microbiol. 144 (2010) 64-71.

5. J.M. Amigo, Practical issues of hyperspectral imaging analysis of solid dosage forms, Anal. Bioanal. Chem. 398 (2010) 93-109.

6. F. Blanco, M. López-Mesas, S. Serranti, G. Bonifazi, J. Havel, M. Valiente, Hyperspectral imaging based method for fast characterization of kidney stone types, J. Biomed. Optics, 17 (2012) 076027-1-076027-12.

7. J.M. Prats-Montalbán, A. de Juan, A. Ferrer, Multivariate image analysis: A review with applications, Chemom. Intell. Lab. Syst. 107 (2011) 1-23.

8. C. Gendrin, Y. Roggo, C. Collet, Pharmaceutical applications of vibrational chemical imaging and chemometrics: A review, J. Pharmaceut. Biomed. 48 (2008) 533-553.

9. A. Plaza, J.A. Benediktsson, J.W. Boardman, J. Brazile, L. Bruzzone, G. Camps-Valls, J. Chanussot, M. Fauvel, P. Gamba, A. Gualtieri, M. Marconcini, J.C. Tilton, G. Trianni,

Recent advances in techniques for hyperspectral image processing, Remote Sens. Environ. 113 (2009) S110–S122.

10. J. Burger, A. Gowen, Data handling in hyperspectral image analysis, Chemom. Intell. Lab. Syst. 108 (2011) 13-22.

11. L. Nørgaard, A. Saudaland, J. Wagner, J.P. Nielsen, L. Munck, S.B. Engelsen, Interval Partial Least-Squares Regression (iPLS): A Comparative Chemometric Study with an Example from Near-Infrared Spectroscopy, Appl. Spectrosc. 54 (2000) 413-419.

12. R. Leardi, Genetic algorithms in chemometrics and chemistry: a review, J. Chemom. 15 (2001) 559-569.

13. Z. Liu, H. Yu, J.F. MacGregor, Standardization of line-scan NIR imaging systems, J. Chemom. 21 (2007) 88-95.

14. J. Burger, P. Geladi, Hyperspectral NIR image regression part I: Calibration and correction, J. Chemom. 19 (2005) 355-363.

15. P. Tatzer, M. Wolf, T. Panner, Industrial application for inline material sorting using hyperspectral imaging in the NIR range, Real-Time Imaging 11 (2005) 99-107.

16. G. Bonifazi, S. Serranti, Imaging spectroscopy based strategies for ceramic glass contaminants removal in glass recycling, Waste Manag. 26 (2006a) 627-639.

17. G. Bonifazi, S. Serranti, Hyperspectral imaging based techniques in fluff characterization, Proc. SPIE 6377, U151-U160, Bellingham, WA, USA DOI: 10.1117/12.684661 (2006b).

18. G. Bonifazi, S. Serranti, Hyperspectral imaging based procedures applied to bottom ash characterization, Proc. SPIE 6755, 0B1-0B8, Bellingham, WA, USA DOI: 10.1117/12.735803 (2007).

19. G. Bonifazi, S. Serranti A. Bonoli, A. Dall'Ara, Innovative recognition-sorting procedures applied to solid waste: the hyperspectral approach, in C.A. Brebbia, M. Neophytou, E. Beriatos et al. (Eds.), Sustainable development and planning IV, Book Series: WIT Transactions on Ecology and the Environment, 120, 885-894. WIT Press, Southampton, Boston, ISBN: 978-1-84564-422-2, doi: 10.2495/SDP090832.

20. A. Kulcke, C. Gurschler, G. Spöck, R. Leitner, M. Kraft, On-line classification of synthetic polymers using rear-infrared spectral imaging, J. Near Infrared Spectrosc. 11 (2003) 71-81.

21. R. Leitner, Real-time classification of polymers with NIR spectral imaging and blob analysis, Real-Time Imaging 9 (2003) 245-251.

22. S. Serranti, A. Gargiulo, G. Bonifazi, Characterization of post-consumer polyolefin wastes by hyperspectral imaging for quality control in recycling processes, Waste Manag. 31 (2011) 2217-2227.

23. S. Serranti, A. Gargiulo, G. Bonifazi, Classification of Polyolefins from Building and Construction Waste using NIR Hyperspectral Imaging System, Resour. Conserv. Recycl. 61 (2012) 52-58.

24. F.P. La Mantia, L. Botta, M. Morreale, R. Scaffaro, Effect of small amounts of poly(lactic acid) on the recycling of poly(ethylene terephthalate) bottles, Polymer Degrad. Stabil. 97 (2012) 21-24.

25. A. Carné Sánchez, S.R. Collinson, The selective recycling of mixed plastic waste of polylactic acid and polyethylene terephthalate by control of process conditions, Eur. Polym. J. 47 (2011) 1970-1976.

26. S. Chevallier, D. Bertrand, A. Kohler, P. Courcoux, Application of PLS-DA in multivariate image analysis, J. Chemom. 20 (2006) 221-229.

27. A. de Juan, R. Tauler, Chemometrics applied to unravel multicomponent processes and mixtures Revisiting latest trends in multivariate resolution, Anal. Chim. Acta 500 (2003) 195-210.

28. M. Forina, P. Oliveri, H. Jäger, U. Römish, J. Smeyers-Verbeke, Class modeling techniques in the control of the geographical origin of wines, Chemom. Intell. Lab. Syst. 99 (2009) 127-137.

29. R. Gosselin, D. Rodrigue, C. Duchesne, A Bootstrap-VIP approach for selecting wavelength intervals in spectral imaging applications, Chemom. Intell. Lab. Syst. 100 (2010) 12-21.

30. A. de Juan, R. Tauler, R. Dyson, C. Marcolli, M. Rault, M. Maeder, Spectroscopic imaging and chemometrics: a powerful combination for global and local sample analysis, TrAC – Trend Anal. Chem. 23 (2004) 70-79.

31. I.G. Chong, C. H. Jun, Performance of some variable selection methods when multicollinearity is present, Chemom. Intell. Lab. Syst. 78 (2005) 103.

32. C.M. Andersen, R. Bro, Variable selection in regression - a tutorial, J. Chemom. 24 (2010) 728–737.

33. D.A. Burns, E.W. Ciurczak (Eds.), Handbook of Near-Infrared Analysis, third ed., CRC Press, Boca Raton, 2008.

TABLES AND FIGURES CAPTIONS

Table 1. PLS-DA Classification Efficiency results obtained with the whole Img1 hypercube and with the corresponding reduced matrix.

Table 2. PLS-DA Classification Efficiency results obtained after variable selection with the whole Img1 hypercube and with the corresponding reduced matrix.

Figure 1. PC1-PC2 scores plot and PC2 score image obtained from PCA performed on merged and meancentered Img0 and Img1 before (a, b) and after (c, d) the internal calibration.

Figure 2. (a) Raw median spectra and (b) corresponding preprocessed (2^{nd} derivative + mean centering) spectra of the three classes calculated on the whole Img1.

Figure 3. Results of PCA applied to Img1. (a): RGB image; (b): PC1-PC2 scores plot showing the cluster-based selection of the 3 selected classes: background (red), PET (green) and PLA (blue); (c): image representation of the three selected classes;

Figure 4. (a) PC1 loading vectors vs. preprocessed median spectrum of PET; (b) PC2 loading vectors plot vs. preprocessed median spetrum of PLA.

Figure 5. (a) VIP scores of the PLS-DA model calculated on the whole Img1 ; (b) variables selected on the whole matrix and (c) on the reduced matrix of Img1 by means of iPLS-DA dividing the spectral range in 7 (A, D), 14 (B, E) and 49 (C, F) intervals.

Figure 6. Img7 andImg 9: (a) acquisition schemes; (b) corresponding RGB images; (c) PLS-DA predicted class probabilities (red for background, green for PET, blue for PLA); (d)

MCR-ALS estimated concentrations (red for component 1, green for component 2, blue for component 3).

Figure 7. Spectra profiles of the three components recovered by means of the MCR-ALS algorithm calculated on the reduced matrix of Img1.

Figure 8. Img4 andImg5: (a) acquisition schemes; (b) RGB images; (c) MCR-ALS estimated concentrations (red for component 1, green for component 2, blue for component 3).

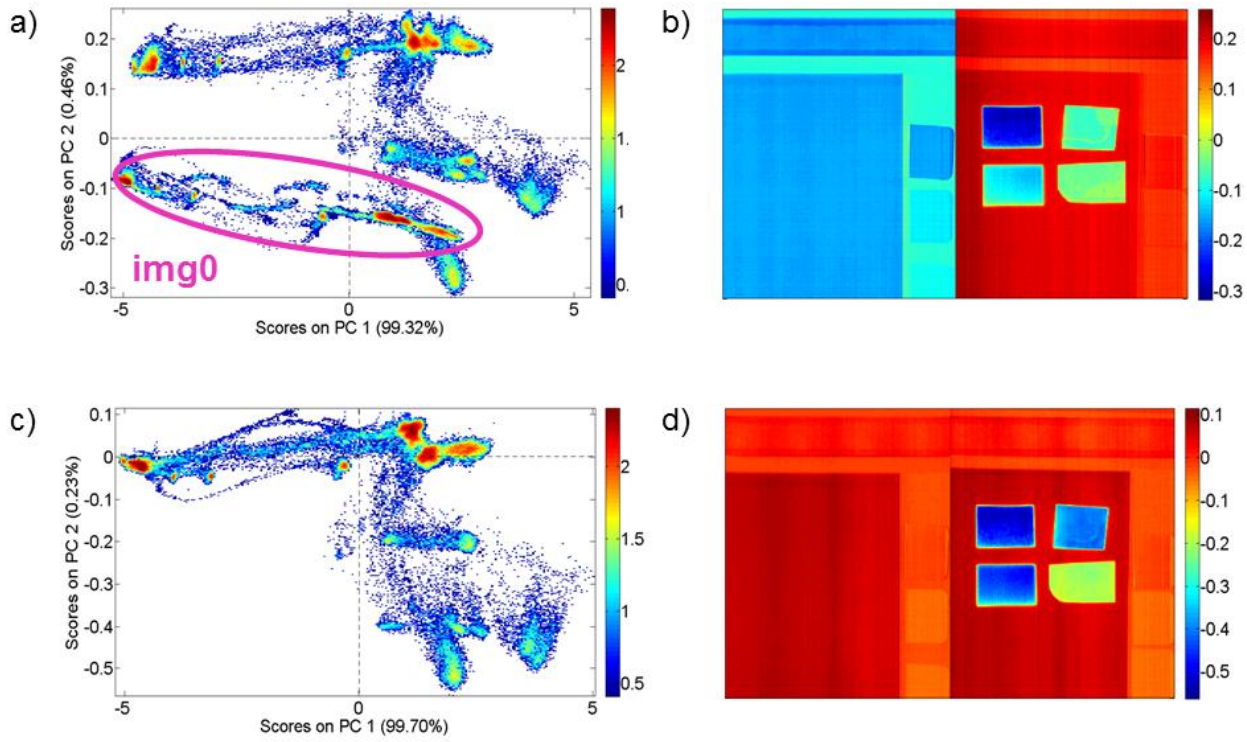

Figure 1

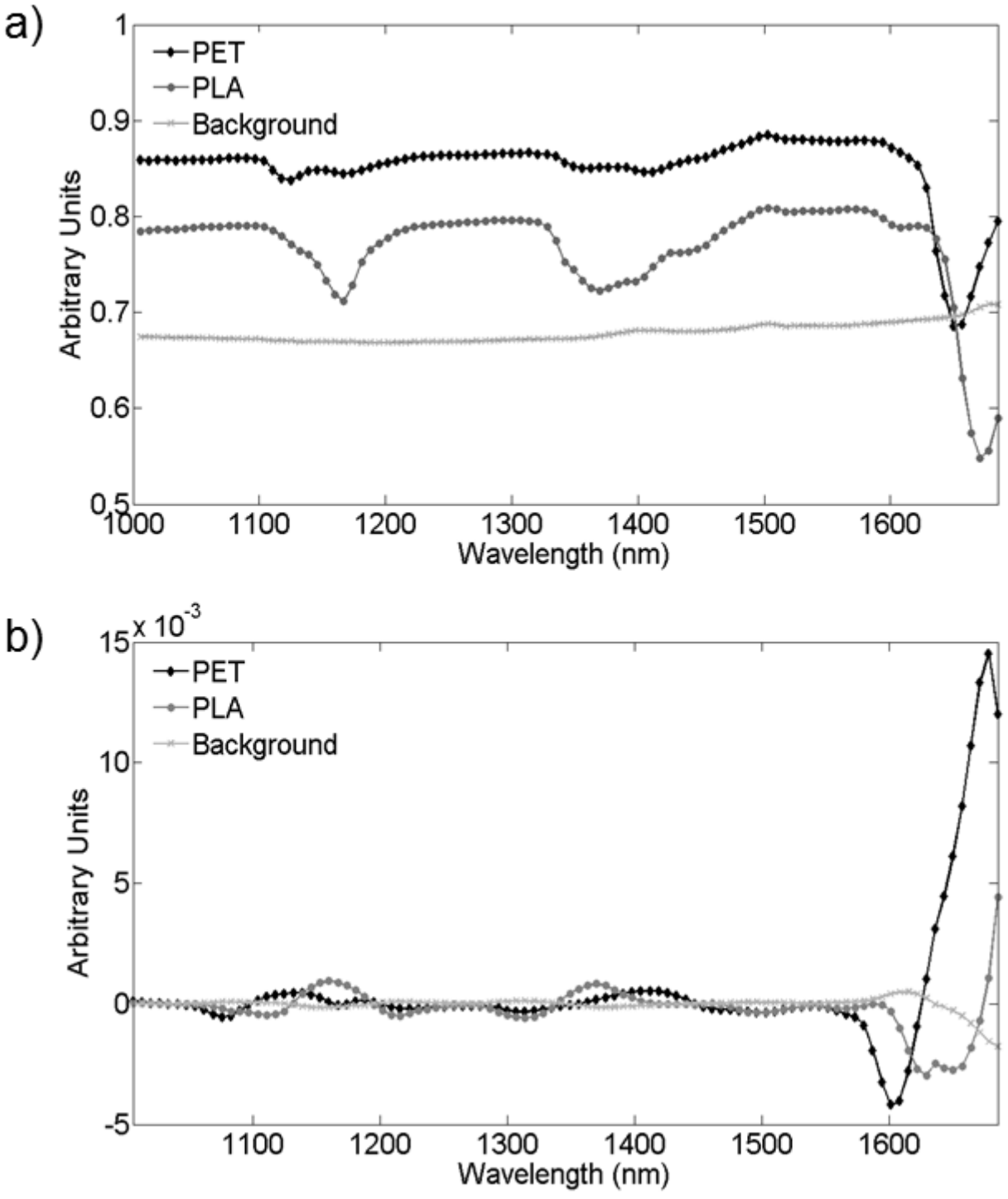
a)
PET
PLA
Background
Arbitrary Units
Wavelength (nm)
b)
x 10^-3
PET
PLA
Background
Arbitrary Units
Wavelength (nm)

Figure 2

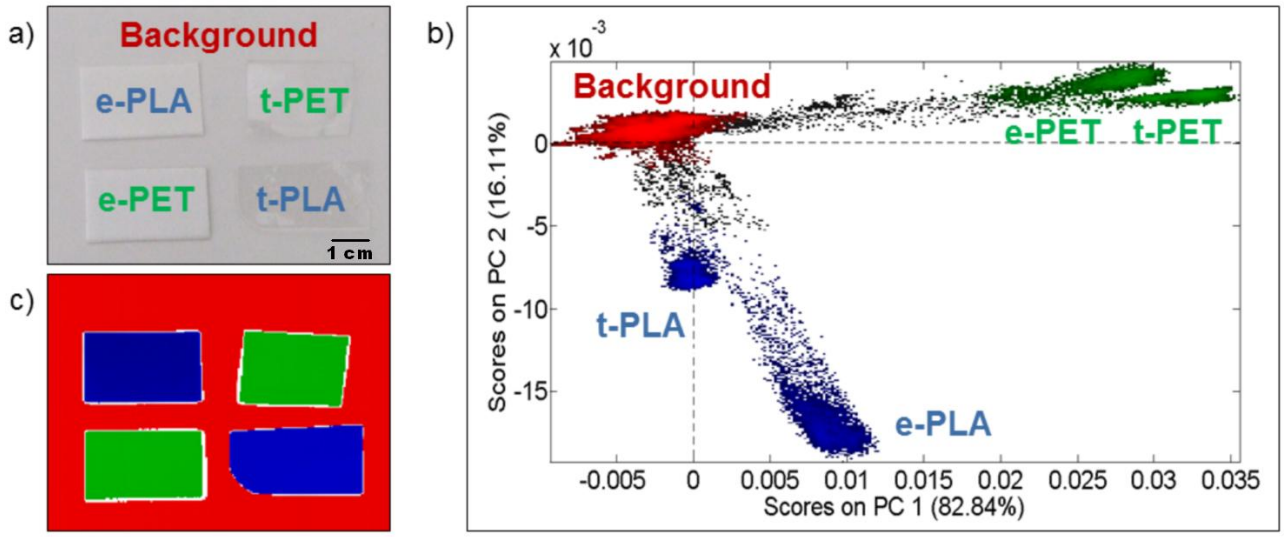

Figure 3

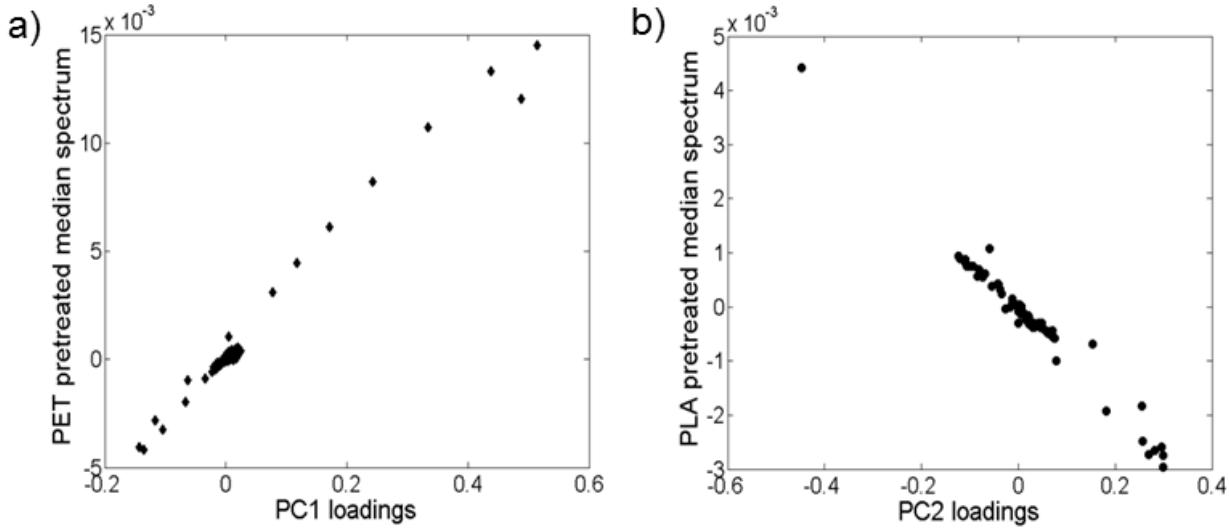

Figure 4

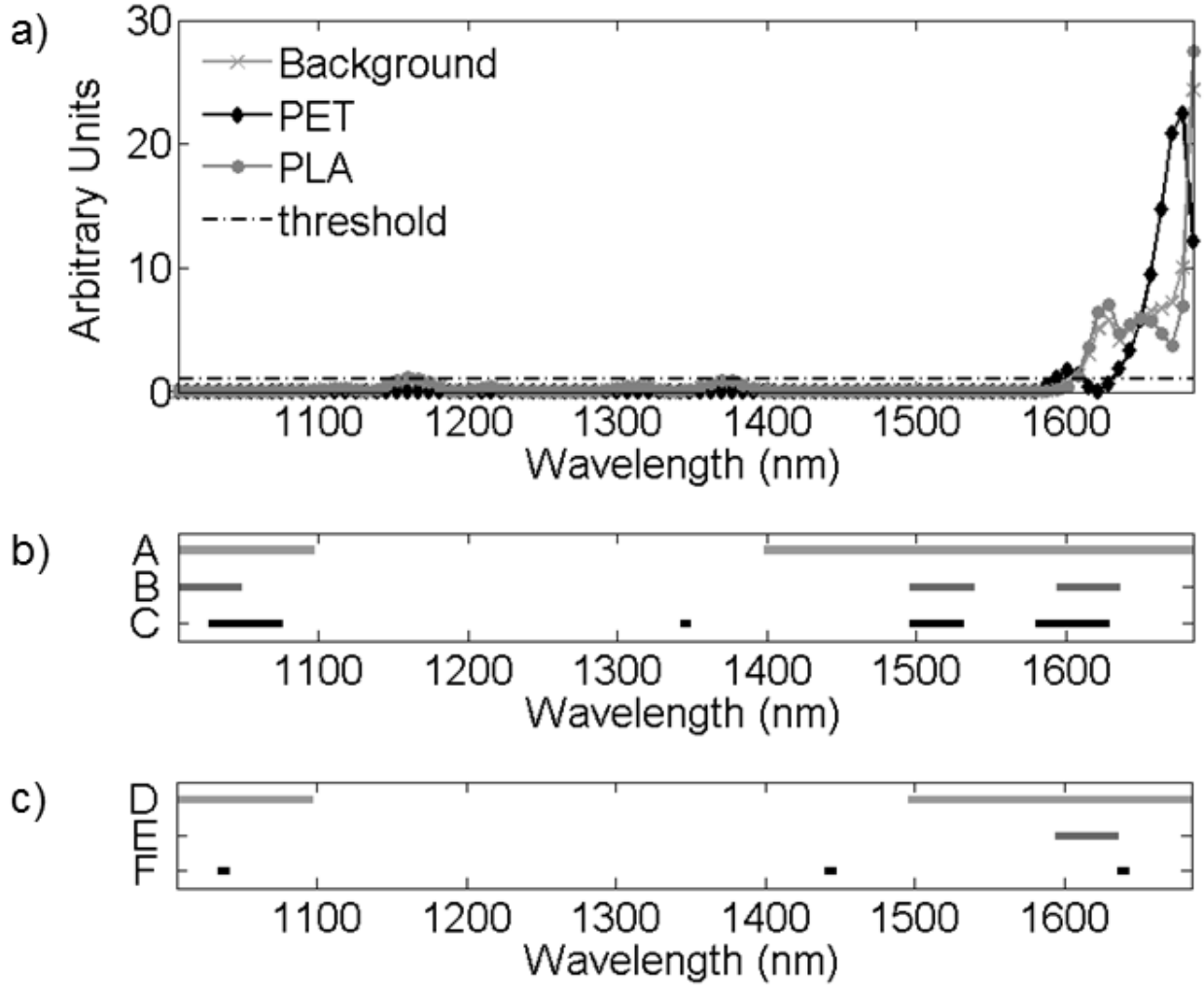
a)
Arbitrary Units
30
20
10
0
Background
PET
PLA
threshold
1100
1200
1300
1400
1500
1600
Wavelength (nm)
b)
A
B
C
1100
1200
1300
1400
1500
1600
Wavelength (nm)
c)
D
E
F
1100
1200
1300
1400
1500
1600
Wavelength (nm)

Figure 5

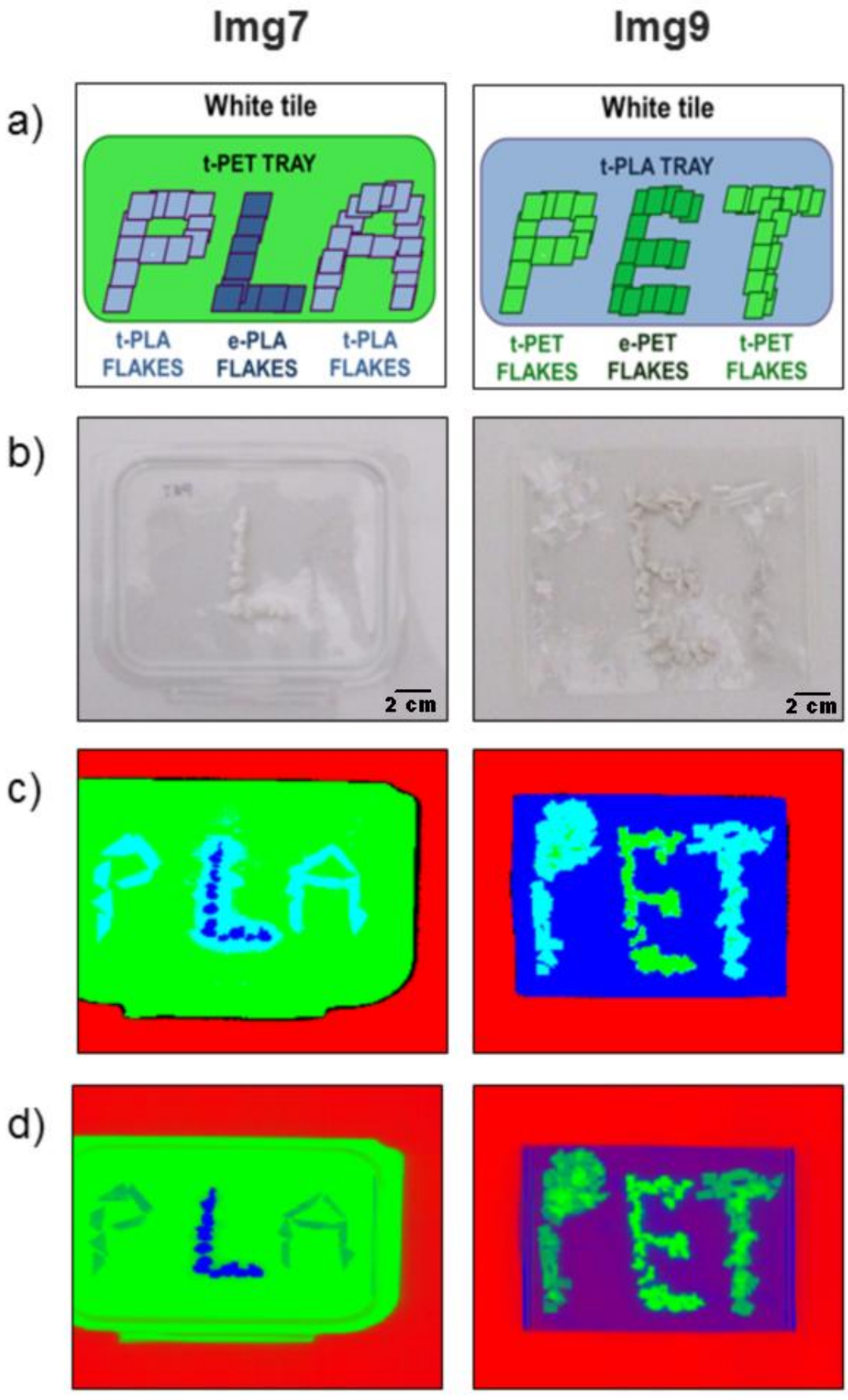
Img7
Img9
a)
White tile
t-PET TRAY
PLA
t-PLA FLAKES
e-PLA FLAKES
t-PLA FLAKES
White tile
t-PLA TRAY
PET
t-PET FLAKES
e-PET FLAKES
t-PET FLAKES
b)
2 cm
2 cm
c)
d)

Figure 6

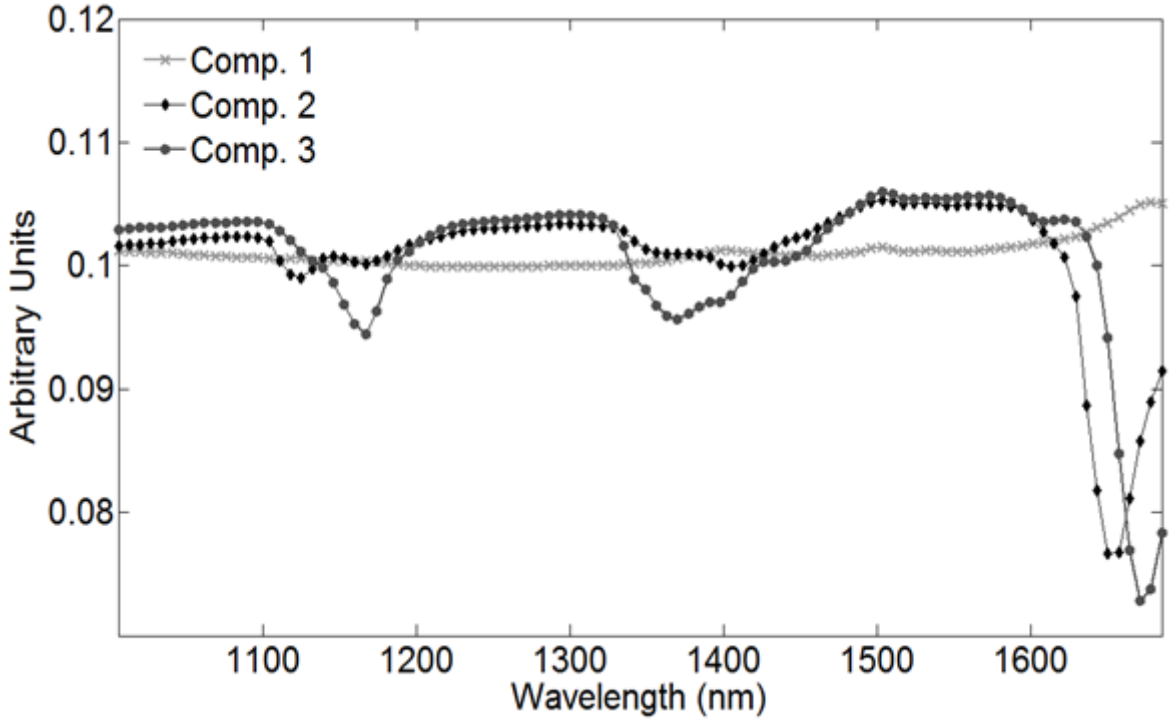

Figure 7

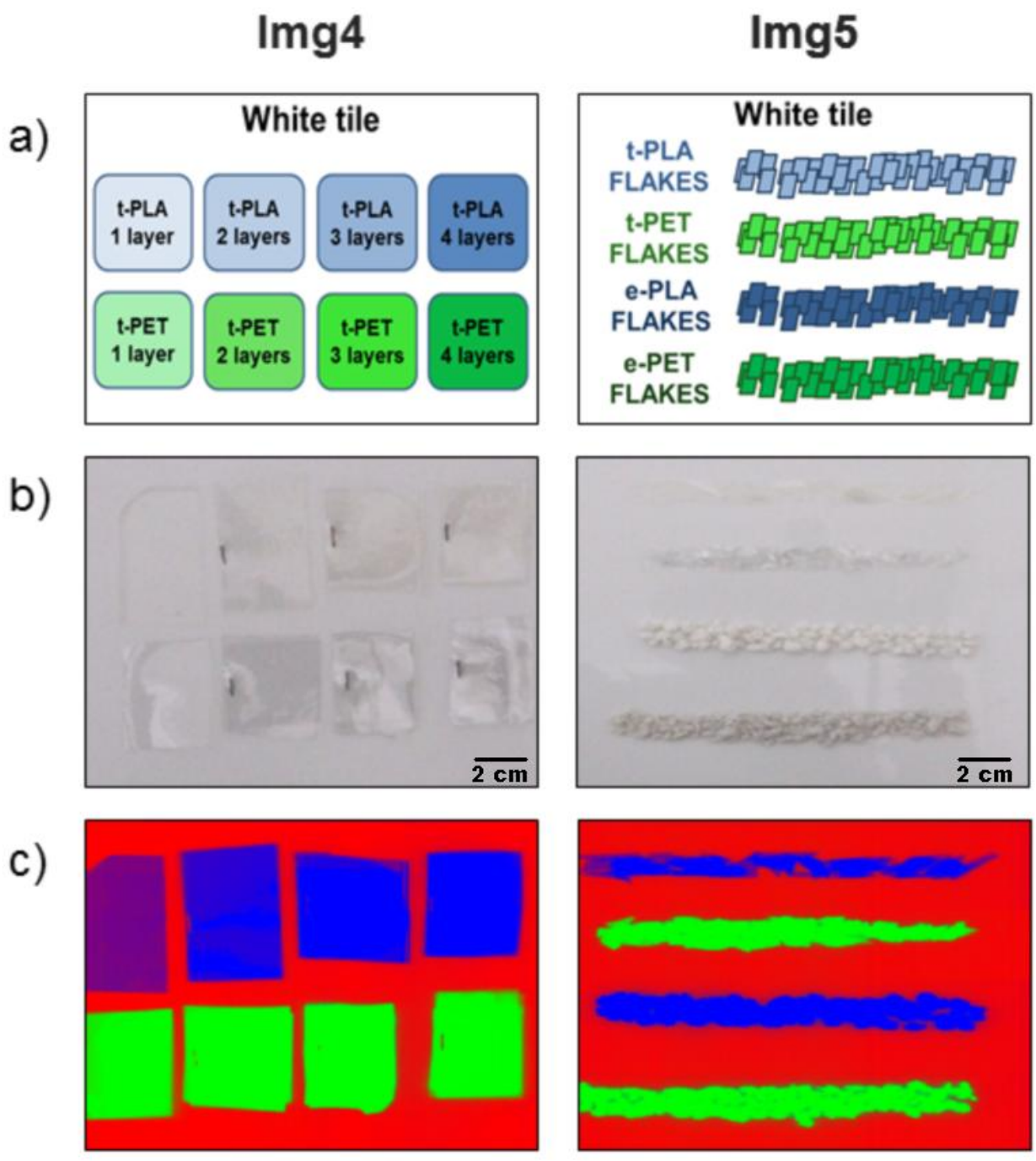

Figure 8

Tables

Table 1

	Efficiency (%) of the PLSDA models					
	Whole matrix			Reduced matrix		
	Background	PET	PLA	Background	PET	PLA
Img1 (CV)	99.85	100.00	99.90	100.00	100.00	100.00
Img2 (Pred)	99.85	100.00	99.95	99.60	100.00	99.95
Img3 (Pred)	99.90	100.00	99.85	99.65	100.00	99.90
Img4 (Pred)	99.50	100.00	99.35	98.94	100.00	99.50
Img5 (Pred)	99.55	100.00	99.10	98.94	100.00	99.25
Img6 (Pred)	98.79	100.00	98.54	98.13	100.00	98.69

Table 2

			Interval size 14		Interval size 7		Interval size 2	
			Whole matrix	Reduced matrix	Whole matrix	Reduced matrix	Whole matrix	Reduced matrix
#° of LVs			2	2	2	2	2	2
#° of selected wavelengths			56	42	21	7	24	6
Calculation time (s)			188	20	242	24	3325	168
Efficiency (%)	Img1 (CV)	Background	99.90	100.00	99.85	100.00	99.90	100.00
		PET	100.00	100.00	100.00	100.00	100.00	100.00
		PLA	99.95	100.00	99.80	100.00	99.85	100.00
	Img2 (Pred)	Background	99.85	99.65	99.85	99.80	99.80	99.90
		PET	100.00	100.00	100.00	100.00	99.95	100.00
		PLA	99.95	100.00	99.95	99.95	100.00	99.90
	Img3 (Pred)	Background	99.90	99.70	99.85	99.80	99.85	99.90
		PET	100.00	100.00	100.00	100.00	100.00	100.00
		PLA	99.95	100.00	99.95	100.00	99.95	99.95
	Img4 (Pred)	Background	99.70	99.25	99.50	99.40	99.40	99.60
		PET	100.00	100.00	100.00	100.00	99.90	100.00
		PLA	99.70	99.90	99.85	99.90	99.80	99.70
	Img5 (Pred)	Background	99.90	99.50	99.10	98.99	98.89	99.65
		PET	99.95	100.00	99.95	100.00	99.45	100.00
		PLA	99.60	99.90	99.85	99.85	99.75	99.95
	Img6 (Pred)	Background	99.20	98.69	98.39	98.23	98.18	98.99
		PET	99.95	100.00	99.80	100.00	99.30	100.00
		PLA	98.99	99.35	99.35	99.40	99.25	99.55

Highlights

- Classification of PET and PLA by NIR-HSI was carried out for recycling purposes
- A new internal calibration procedure allowed to optimize image reproducibility
- An efficient data compression strategy was developed (max compr. ratio = 3×10^-4)
- PLS-DA, iPLS-DA and MCR-ALS were applied to distinguish PET from PLA
- PET and PLA were correctly identified, also using the compressed datasets